Performance of the double delay line microchannel plate detectors for the Far Ultraviolet Spectroscopic Explorer

Oswald H.W. Siegmund, Mark Gummin, Geoffrey Gaines, Giampiero Naletto,
Joseph Stock, Richard Raffanti, Jeffrey Hull, Robert Abiad, Ted Rodriguez-Bell,
Tony Magoncelli, Patrick Jelinsky, William Donakowski, and Karl Kromer
Experimental Astrophysics Group
Space Sciences Laboratory
University of California
Berkeley, CA 94720

Phone 510-642-0895, Fax 510-643-9729
email, ossy@ssl.berkeley.edu

ABSTRACT

The microchannel plate, delay line, detectors developed for the Far Ultraviolet Spectroscopic Explorer[1] mission to be launched in 1998 are described. The two FUSE detectors have a large format (•184mm x 10mm split into two 88.5 x 10mm segments), with high spatial resolution (<20µm x 50µm FWHM, >9000 x 200 resolution elements) and good linearity (±25µm), high image stability, and counting rates in excess of 4 x 10^4 events sec^{-1}. KBr opaque photocathodes have been employed to provide quantum detection efficiencies of 30-40% in the 900 - 1200Å range. Microchannel plates with 10µm pores and an 80:1 pore length to diameter ratio, with a 95mm x 20mm format have been used in a Z stack configuration to provide the photon amplification (gain • 2 x 10^7). These show narrow pulse height distributions (<35% FWHM) even with uniform flood illumination, and good background levels (<0.3 event cm^{-2} sec^{-1}). Flat field images are dominated by the microchannel plate multifiber boundary fixed pattern noise and are stable.

Keywords: ultraviolet, spectroscopy, microchannel plate

2. FUSE DETECTOR SUBSYSTEM

2.1 FUSE instrument

The FUSE optical configuration consists of four normal incidence •36cm mirrors in combination with four gratings providing two LiF, and two SiC channels to cover the bandpass •905Å to 1190Å. The spectra produced are imaged on two separate detectors, each one reading out the spectra of two optical paths that are separated by displacing them in the cross dispersion direction. The gap between the spectra also allows off target sky background spectra to be obtained. The spectral resolution needed for the mission objectives is $\lambda/\delta\lambda$ = 30,000, form which we derive a focal plane detector that is 184mm in length and 10mm high, curved to a 0.826m (± 50µm) radius to match the Rowland circle of the optics. Basic requirements for the FUSE detectors that result from the science goals and the instrument performance requirements are: a resolution of •17µm FWHM in X (dispersion direction) and <50µm FWHM in Y (cross-dispersion direction), quantum detection efficiency (QDE) •30% over the range 905 to 1190Å, counting rate capacity of >4 x 10^4 events sec^{-1}, with low image distortion, fixed pattern noise <10%, high operational stability, and the robustness to withstand launch without changes in operating characteristics.

Based on performance data with large format detectors (ORFEUS[2] and rockets), microchannel plate detectors with delay line readouts have been chosen for FUSE. We have adopted a helical multiplanar double delay line readout system for the detector, segmented into two sections to achieve redundancy and to attain the resolution and format required (•10,000 FWHM resolution elements). The resulting detector subsystem consists of two focal plane detectors with front end electronics, & a pair of main electronics packages for the command & signal processing electronics.

2.2 Detector subsystem components

The FUSE detector subsystem (Fig. 1) consists of two main parts. The first is a vacuum housing containing the detector with front end amplifiers and high voltage filter module attached, a +15V grid (95% transmission) over the entrance aperture, a pair of ion pumps and a motor driven reclosable door mechanism. The 4l/s ion pumps are being used only for pre-flight tests to maintain low pressures (<$2x10^{-6}$ Torr), and to preserve the photocathode efficiency. The detector housing door can be opened remotely during full instrument vacuum chamber testing. Two sapphire windows in the door (one for each segment) can also be used for stand alone tests with the door closed. The second, the main electronics package (Fig. 1), consists of high voltage and low voltage power supplies, X time to digital converters and Y charge to digital converters for signal processing electronics and a data and houskeeping interface/controller. The high voltage supplies also supply the power for the ion pumps and the +15v ion grid.

2.3 Detector configuration and operation

The FUSE detector design is shown in Figure 2 and consists of two individual 88.5mm x 10mm sensor segments, separated by •7mm, that are independently operable, but within a single integrated detector body subassembly. A 95% transmission electroformed Ni mesh with two segments is mounted on an insulating mount •6mm above the MCP stack to deflect photoelectrons back down onto the MCP's. Each detector segment comprises of an opaque photocathode deposited on a cylindrically curved (0.826mm) MCP Z stack. The MCP's are held in the brazed metal-ceramic detector body using a circumferential spring clamp and curved pressure pad. This has been proven to maintain the MCP radius of curvature to within 50µm of the required shape, and is repeatable on disassembly/reassembly to 25µm. Photon event positions are read out with a delay line anode and associated electronics. Incoming photons interact with the photocathode, resulting in photoelectron emission. The photoelectrons impact the walls of MCP pores causing a charge avalanche, giving an overall charge multiplication of >10^7. This charge cloud is drifted over the •6mm gap from the MCP output to the delay line anode. The readout anode and the brazed detector body are attached to the vacuum flange, containing both signal and high voltage feedthroughs, to which the amplifier electronics box and HV filter module are also attached. The charge dumped on the anode is divided by the delay line electrodes so that Y event positions may be deduced from the ratio of charges on two wedge shaped electrode sets, and the X event positions are deduced from the signal arrival time differences at the two ends of the anode. Image encoding electronics provides the necessary algorithms for event position determination, and digitizes the X and Y event positions prior to data histogramming and/or telemetry to the ground. The overall delay line detector scheme is similar to those we built & have successfully flown on the ORFEUS[2] payload in 1993 and 1996 on the Shuttle.

2.3.1 Photocathode configuration

The photocathode configuration is shown in Figure 6. A KBr photocathode is applied to the front of the MCP's by evaporation, coating the MCP's at an angle of •5° to the pore axis and rotating the MCP during deposition. The biased mesh directly above the microchannel plate stack is used to further enhance[3,4] the QDE by deflecting emitted photoelectrons back down onto the MCP. KBr provides both high QDE and long term stability[5] as demonstrated on our measurements of other KBr test photocathodes, and application of KBr photocathodes on the EUVE and ORFEUS instruments.

2.3.2 Microchannel plates

FUSE employs a MCP Z stack providing high gain (>10^7) and low background, curved to match the focal surface of the Rowland spectrograph. The two detector segments each employ a 95mm x 20mm MCP Z stack curved to the 0.826m radius. The performance characteristics of MCP Z stacks (gain • 2 x 10^7, pulse height <50% FWHM, background rate (<0.5 events cm^{-2} sec^{-1})[6], and event rate capability (>10 events $pore^{-1}$ sec^{-1})[5]) meet the requirements for FUSE, & have been demonstrated by their use in instruments such as EUVE, ORFEUS[7], FAUST, & rockets.

A variety of MCP's were obtained for the FUSE program. All the MCP's were produced with cylindrical curvature generated by thermal slumping. MCP's from Galileo in both low noise glass, and long life glass were procured. These have pore sizes of 10µm on 12µm centers, 12° bias angle, 80:1 channel length to diameter ratio (L/D), and resistances in the range 20M• to 100M•. MCP's procured from Philips have pore sizes of 10µm on 12µm centers, or 12µm on 15µm centers, 13° bias angle, 80:1 channel length to diameter ratio (L/D), & resistance in the range 15M• to 100M•.

MCP's with the lower values (<40M•) were selected for flight since the local event rate capacity is higher for low resistance MCP's [8]. The background rate is normally dominated by the radioactive β decay in the MCP glass [6,9] . The Philips MCP's and the Galileo low noise glass meet the FUSE requirements, while the Galileo long life glass contains rubidium resulting in a higher [6,9] background rate. Other issues affecting the selection of MCP's for flight include the quantum efficiency, the incidence of background hot spots, and the MCP pore size and fixed pattern noise.

A number of difficulties were experienced in the production of the MCP's for FUSE which resulted in the use of an unconventional MCP arrangement. To achieve the spectral resolution required and low levels of small scale fixed pattern noise, along with high quantum efficiency and low background rates, we have implemented MCP Z stacks using a 10µm pore MCP/12µm pore MCP/10µm pore MCP configuration. The details of the MCP performance evaluations are discussed in the presentation of the test results.

2.3.3 Delay line anode design

The combination of resolution, large size, curved focal plane, and counting rate performance for the FUSE detectors presents a considerable challenge for the readout anode. We have developed a helical multiplanar double delay delay line (HDDL) anode (Fig. 3) for the FUSE mission. HDDL anode formats are ideal for applications in spectroscopy instruments, where the cross-dispersion axis (Y) is shorter than the dispersion axis (X), and high spatial resolutions are needed for the dispersion direction. To accomodate the two detector segments, two separate anodes have been fabricated for each detector and positioned end to end (Fig. 3). The active area for each anode is 15mm x 94mm, with abutted multiplanar helical delay lines 25mm tall both above and below the active area (Fig. 3, 4). The MCP charge pulse (•3 to 5 ns width) is detected on, and divided between, two sets of conductive wedges (Fig. 4), so that the Y event centroid coordinates may be determined from charge ratios of signals on opposing wedge sets. Each wedge set is connected to external delay lines which extend across the anode top and bottom surfaces and are connected by plated through holes to form a helical configuration (Fig.4). The X photon event centroid is determined from the difference in arrival times of the event signal at the two anode ends. The anode substrate (RT Duroid) has high permittivity which controls the pulse propagation speed. Typical end to end delay times are •100ns for the FUSE HDDL anodes 94mm long in X with •0.5mm period and delay line helixes •25mm high. Thick Cu conductors and a substrate with low loss coefficient minimize the pulse attenuation and dispersion as it travels across the anode.

The HDDL anodes are produced by photolithographically etching the anode patterns into conductor layers deposited on low loss flexible microwave substrates. (6010 RT/Duroid substrates, ceramic doped PTFE, ε •10.5, loss coefficient 0.0023 @10 GHz, 250µm thick dielectric coated with •30µm Cu on both sides). The delay line comprises two substrates that include a center (buried) ground plane between the top and bottom parts of the helical delay line. These are bonded together and connected by through plating of the interconnect holes (Fig. 4). The final anode is connected to the signal feedthroughs with gold plated pogos, and is mounted onto a curved substrate to match the MCP curvature.

2.3.4 Imaging electronics

The position encoding electronics for the FUSE detector is shown schematically in Fig. 5. Signals from the anode have a width of •5ns and an average of 1×10^7 e^- per delay line. These signals are processed by two electronic chains to derive the X and Y event centroid positions. The X position encoding electronics begins with a fast timing amplifier chain containing a low pass filter (•120MHz) to optimize the pulse shape and signal to noise ratio. Two of these amplifiers in shielded boxes are mounted to the detector flange (Fig.1) (one per segment). The Y axis encoding electronics has charge sensitive preamplifiers followed by gated integrator shaping amplifiers. The gated integrators provide a short dead time and no loss of spatial resolution at the higher

counting rates. These are packaged in shielded boxes (2 per detector) and mounted beside the fast timing amplifiers.

The fast timing amplifier signals for each detector segment are routed to the time to digital converter card in the main electronics package. A constant fraction discriminator (50% fraction) is used to produce timing signals for each end of the delay line. One signal is delayed, using a lumped delay module, by >100ns to ensure the "start" pulse always precedes the "stop" signal. The time difference between these "start" and "stop" signals are converted to analog voltages by a time to amplitude converter. Subsequently the analog voltage pulses are digitized by a 14 bit (AD7885, 5.3µs convert) analog to digital converter (ADC). Potential problems with the differential non-linearity (DNL) of the ADC causing variations (±50%) in the width of the least significant bit are avoided by using a digital "dither". This technique involves adding a known voltage to the ADC input & then digitally subtracting it at the ADC output. Since the voltage is varied from event to event this has the effect of averaging the ADC DNL over a number of channels. 14 bit electronic binning in X allows position encoding of •6µm to be achieved, oversampling the intrinsic detector point spread function (•15-20µm) on each segment.

The Y event centroid coordinates are determined in the following way. The gated integrator signals are routed to a charge to digital converter board (CDC) in themain electronics package. Here 12 bit ADC's (AD7886, 1µs convert) and a hardware sum and divide calculate Y from the amplitude ratios of the pulses. Since the events from any specific point on the anode vary in amplitude over the range of the MCP pulse height distribution, the Y ADC is effectively already "dithered". Only 10 bits of the Y position data are actually used, however.

Both X and Y digitized data for each photon are passed through a FIFO and linked to the to the instrument data system using an RS422 interface. The pulse amplitude sum signal is separately inserted into the housekeeping data. For verification testing of the electronics there is also a stimulation pulse generator which provides pulses capacitively coupled into the inputs of the preamplifiers resulting in two spots, one at each end of a segment. These provide useful data on the position, relative resolution and stability of the detector system in pre-flight and flight conditions.

2.3.5 Data processing unit &power supplies

The data from the imaging electronics (CDC's, & TDC's) is transferred to the FUSE instrument data system via an RS422 interface, where it is packaged and formatted for telemetry. The types of data format include photon lists of X, Y photon positions and pre-binned image histogams, the latter being used for high counting rate sources where high signal to noise ratios are expected. The detector data processing unit performs the dual functions of commanding the detector functions and passing back houskeeping data to the FUSE data system via a MIL-1553 interface. Specific command functions include the high voltage levels and amplitude and timing thresholds to each detector segment, opening and closing of the door, stimulation pulser and stimulation lamp control, and SAA/count rate protection limits, and image mask definition. The stimulation lamp is a mercury vapor lamp which will be mounted above the detector in the instrument to provide a global illumination for verification tests in orbit. The image mask functions are provided to accomodate observations with global counting rates that are too high. Arbitrary software masking af any specific area of the detector can be accomplished so that only specific areas of interest are placed in limited space available in the telmetry stream. The houskeeping data includes numerous parameters, such as the high voltage level and current, temperatures, door status, threshold settings, count rates, etc. The DPU boards are mounted alongside the CDC's and TDC's in the main electronics package.

The low voltage DC power supply and high voltage power supply (HVPS) are also mounted on the main electronics package. Fig. 1 shows the main electronics package is composed of essentially identical boxes stacked up containing the DPU, HVPS, LVPS, CDC and TDC for each detector segment. The LVPS conditions the +28v bus power to provide regulated power for the detector imaging electronics and HVPS. The HVPS comprise two units, the main power supply, & the filter module which is mounted on the detector flange. These work in unison to provide three voltage levels to each detector segment, the MCP to anode bias which is fixed, the HV across the MCP stack which is adjustable for gain trimming, and the grid to MCP potential which is fixed and floats above the MCP input voltage.

3. DETECTOR PERFORMANCE TEST RESULTS

3.1 Quantum detection efficiency

The KBr photocathodes used for FUSE were made using our standard techniques[3,4]. However, although the photocathodes produced were representative of "normal" KBr, we found that problems occured relating to the efficiency of the MCP's onto which they were deposited. The majority of the low noise MCP's received from Galileo, and the 12µm MCP's from Philips were all lower in quantum detection efficiency (QDE) than normal bare MCP's by 25% to 50%. This is not unique in that we have obseved this problem before[8] on other programs. The real issue is that the QDE is also proportionally lower for the photocathode put down onto the MCP. Our investigations have indicated that this is likely to be related to a reduction in the detection efficiency for the primary photoelectrons ejected as the result of photoemission. The problem is most severe at wavelengths where only one or two photoelectrons are emitted from the cathode. The effect has also been observed for flat MCP's in addition to these curved MCP's, so we do not believe that the processing changes to slump the MCP's are explicitly responsible for the deficiency. For FUSE the selection of high QDE MCP's was critical. There is also a potentially serious problem for future missions, and is thus the subject of ongoing investigations.

The FUSE detectors were equipped with Philips low resistance 10µm pore MCP's as the front of the stacks. These had close to normal QDE characteristics and could be matched with a variety of other MCP's. The KBr photocathodes produced were evaluated for their QDE by comparision with standard NIST EUV and FUV photodiodes according to established procedures. The measured results are shown in Fig. 7. The performance is not as good as we had hoped, and is unconventionally low in the 900Å to 100Å regime, but achieves •40% QDE @ 1150Å.

3.2 Microchannel plate performance

The MCP stacks chosen for flight were derived by a process of selection on the basis of parameters such as QDE, background, gain, gain uniformity, pulse height, fixed pattern noise and stability. The result was sets comprised of a 10µm pore MCP at the top of the stack, a 12µm pore MCP in the center, and a 10µm pore MCP on the bottom. Top and middle MCP's were Philips MCP's (since the only 12µm MCP's were provided by Philips) and the bottom MCP's were normally Galileo MCP's. Some combinations were not used due to deficiencies in some MCP batches. For example all of one batch of Philips 10µm pore low resistance MCP's had localized hot spots and were unusable as top MCP's. The Philips 12µm MCP's were also not used as top or bottom MCP's due to possible resolution and long term stability issues.

As might be expected with large MCP stacks which are also curved we had expected potential problems with the gain uniformity and PHD performance. Although some of these problems were encountered many of the stacks gave extremely good performance. Gains of 1×10^7 to 2×10^7 are regularly achieved, with pulse heights of <35% for the fully illuminated detector segment (Fig. 8 & 9). Over much of the segment length the gain variations were <10%, with larger deviations, as expected, at the ends. Much of this behavior is related to the curvature matching of the three MCP's & the way they were clamped, but there were also indications of intrinsic gain variations in the individual MCP's.

Unfortunately, the low noise (low radioactivity) MCP's from Galileo were not used as the top MCP's due to QDE problems. However, separate tests[8] have shown that they provide substantial improvements in the background rate. The MCP's at the top of the stack essentially define the intrinsic background rate in the laboratory. The MCP's used achieve an overall background rate (Fig. 10) of •0.35 events cm^{-2} sec^{-1} with a 15% modal gain threshold, which is in accord with the intrinsic MCP K^{40} β decay in the glass [6,9]. We expect the rate to increase by about a factor of two in orbit due to the cosmic ray contribution.

3.3 Imaging characteristics

3.3.1 Event rate stability

The overall event handling capacity is determined by two issues, one is the effective global event processing dead time of the electronics, and the other is the localised event capacity of the MCP's. The latter has been extensively discussed previously[8] and is essentially determined by the MCP resistances, which were •25-30M•, allowing rates of >5 counts $pore^{-1}$ sec^{-1} to be achieved. The majority of FUSE observations will have counting rates <1000 events sec^{-1} per segment, and for bright objects the telemetry rate is not sufficient for large photon

list files. Therefore the required global rate handling capability is not very high. We have designed the system to allow input rates up to •5 x 10^4 sec^{-1} to be processed. The dead time curve is shown in Fig 11, and is accurately predictable and stable for a given detector segment, although the interaction of all four segments with the instrument data system has yet to be examined. At the highest counting rates the electronics has also been carefully adjusted so that there are essentially no position drifts as a function of event rate.

3.3.2 Resolution and linearity performance

To evaluate the resolution we have employed a pinhole mask with 10µm holes on 1mm x 1mm centers in contact with the top MCP. An image of a pinhole mask on one detector segment is shown in Fig. 12. The performance of the detector at high resolution can only be evaluated by examining the data at full digital resolution, such as that displayed in Fig.13. Values for the point spread functions (Fig. 14) are as small as 15µm FWHM in X (electronic binning is •6µm) and 45µm in Y. Resolution of delay line anodes of this type is determined[10] by the event timing error for the X coordinate, and the charge amplifier noise and partition noise for the Y coordinate. The timing error includes signal attenuation and dispersion, preamplifier noise, discriminator walk and jitter , TAC noise, and ADC errors which amount to •20ps total FWHM for the FUSE electronics. Thus the predicted limiting electronic resolution for FUSE is •10µm FWHM, & confirmed by stimulation pulse tests. The actual operational performance is somewhat more difficult to evaluate due to scale factors & pinhole mask/MCP pore phasing.

The image linearity measured using the centroid positions of images of the test-mask pinholes is shown in Figure 15. The position deviations are typically less than ±25µm, but also have a small (25µm) scale length variation across the anode (curve in the mean of the plot). The position errors are due to several effects, including the mask pinhole fabrication position error (•10µm) and the expected •10µm jitter due to MCP pore position uncertainty with respect to the pinhole locations. In some cases two pores are illuminated by a pinhole, rather than one, thus affecting the apparent resolution. A histogram of all the pinhole image FWHM's in X is shown in Fig. 16. The peak resolution of •16µm is not much larger than the 12.5µm pore separation. Examining the X FWHM's as a function of X position (Fig. 17) it is clear that the resolution is best in the center of the detector. The degradation towards the ends of the field of view may have a combination of causes. The settings for the walk and thresholds are more important in these areas due to the effects of attenuation and dispersion on the anode. In addition it is difficult to keep the mask in exact contact with the MCP, so diffraction and parallax effects may also be contributing.

3.3.3 Flat field performance

The fixed pattern uniformity of the FUSE detectors was evaluated by flooding the detector with a Hg or a Kr lamp. One example shown in Fig 18 is a full flood image which was taken with high statistics (>5 x 10^8 counts) using somewhat non-uniform illumination. The "flat field" is dominated by the MCP multifiber modulation effects. The MCP gain map as a function of position (Fig. 19) also shows that the gain at the MCP multifiber boundaries changes, and that there are small gain variations over large distance scales. Figure 20 shows the flat field response of a small section of the detector. At this level much more detail can be seen, as well a few dark spots due to defects in the MCP's. As a comparison high resolution flat fields with MCP stacks all having the same pore size suffered considerably from Moire effects (Fig.21, 23). The hexagonal modulation pattern has •10% modulation (Fig. 22) due to the bottom MCP of the stack[11], and implies charge cloud deflections occur close to multifiber boundaries. This flat field "fixed pattern noise" is essentially stable and may be "divided out" of observational data[11]. However, at high resolutions such as obtained for FUSE this must be carefully done to avoid mis-interpretation of spectral line data. For a large detector format like FUSE, the amount of time and data required (>10^{10} photons at 16384 x 1024 bins) to accomplish a statistically significant flat field characterisation would be excessive. A more practical method is progressively shifting the spectra during observations to accomplish a "dithering" effect, then to remove the local fixed pattern noise with image deconvolution techniques[12].

Acknowledgments

This work was supported by Johns Hopkins University contract # 8601-02306. Many thanks are extended to the Space Sciences machine shop and the undergraduates who contributed to this project.

References

1. Moos,W. and Friedman, S., *Extreme Ultraviolet Astronomy*, Malina and Bowyer, Eds., Pergamon Press, p. 457, (1991).
2. Hurwitz, M., and S. Bowyer, *Extreme Ultraviolet Astronomy*, Malina and Bowyer, Eds., Pergamon Press, p. 442, (1991).
3. Siegmund, O.H.W. E. Everman, J. Vallerga, J. Sokolowski, and M. Lampton, *Applied Optics*, **26(17)**, 3607 - 3614 (1987).
4. Siegmund, O.H.W. and G. Gaines, Proc. SPIE, **1344**, 217-227 (1990).
5. Siegmund, O.H.W. M.A. Gummin, J. Stock and D. Marsh, ESA symposium on detectors, **ESA SP-356**, (1992).
6. Siegmund, O.H.W., Vallerga, J., and Wargelin, B., *IEEE Trans. Nucl. Sci. ,* **NS-35,** 524 (1988).
7. Stock, J. O.H.W. Siegmund, M. Hurwitz, R. Raffanti, S. Bowyer, & M. Lampton, *Proc. SPIE*, **2006**, 128-138 (1993).
8. Siegmund, O.H.W. M.A. Gummin, T. Ravinett, S.R. Jelinsky, & M. Edgar, *Proc. SPIE*, **2808**, 98-106 (1996).
9. Fraser, G.W., Pearson, J.F., and Lees, J.E., *Nucl. Instrum. & Meth.*, **A254**, 447 (1987).
10. Siegmund, O.H.W., Lampton, M., and Raffanti, R., *Proc. SPIE ,* **1159,** 476 (1989).
11. Vallerga, J.V., Siegmund, O.H.W., Vedder, P.W., Gibson, J., *Nucl. Instrum. & Meth*. **A310**, 317-322 (1991).
12. Sahnow, D. J., C. W. Bowers, O. H. W. Siegmund, J. Stock, and M. A. Gummin, *Proc. SPIE,* **1945**, April, (1993).

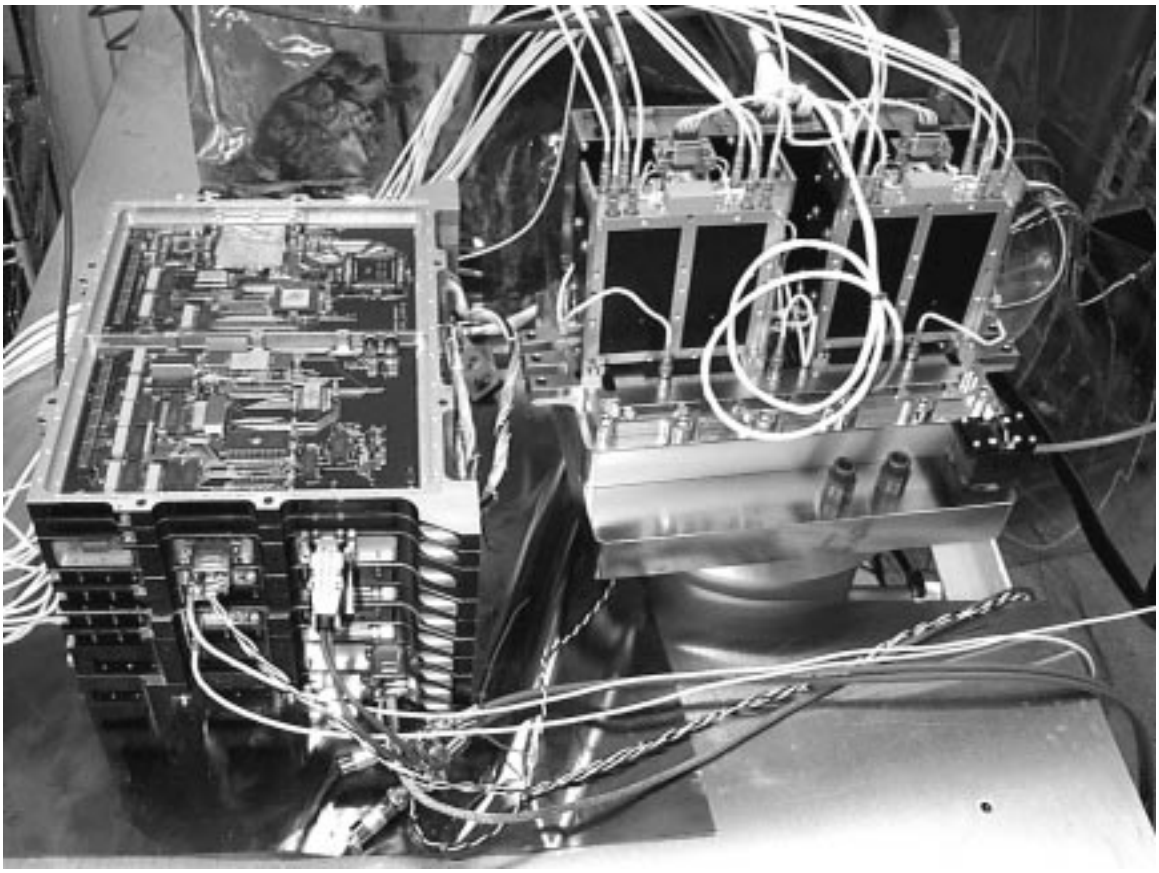

Figure 1. FUSE detector system showing the detector flange with amplifiers and main electronics stackup

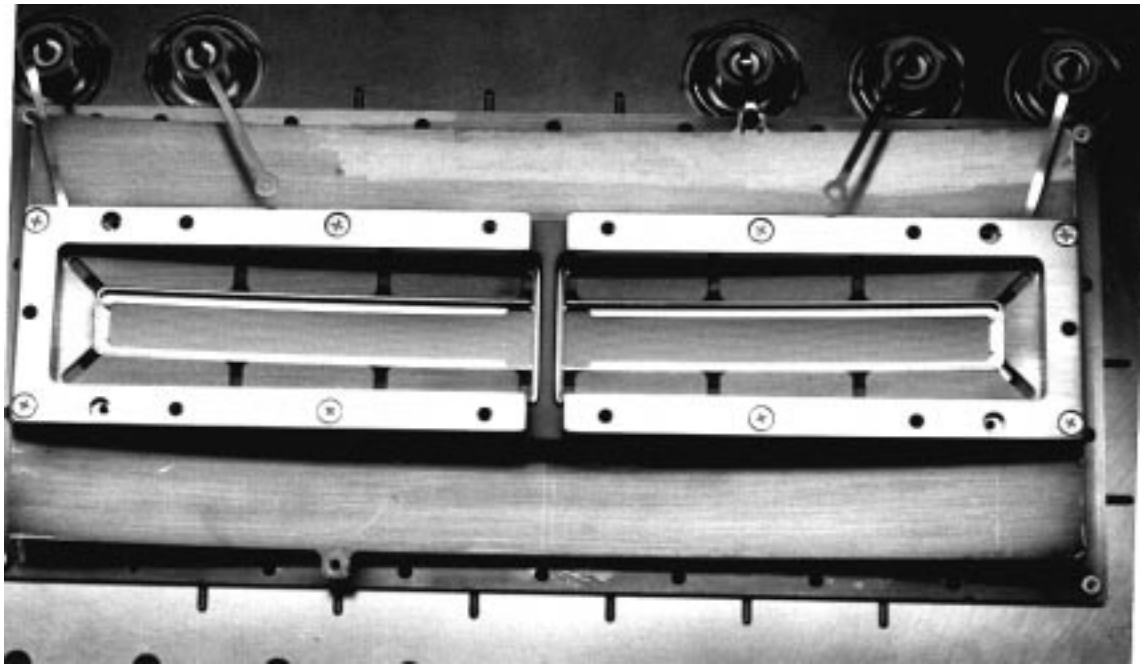

Figure 2. FUSE detector showing the two cylindrically curved MCP segments

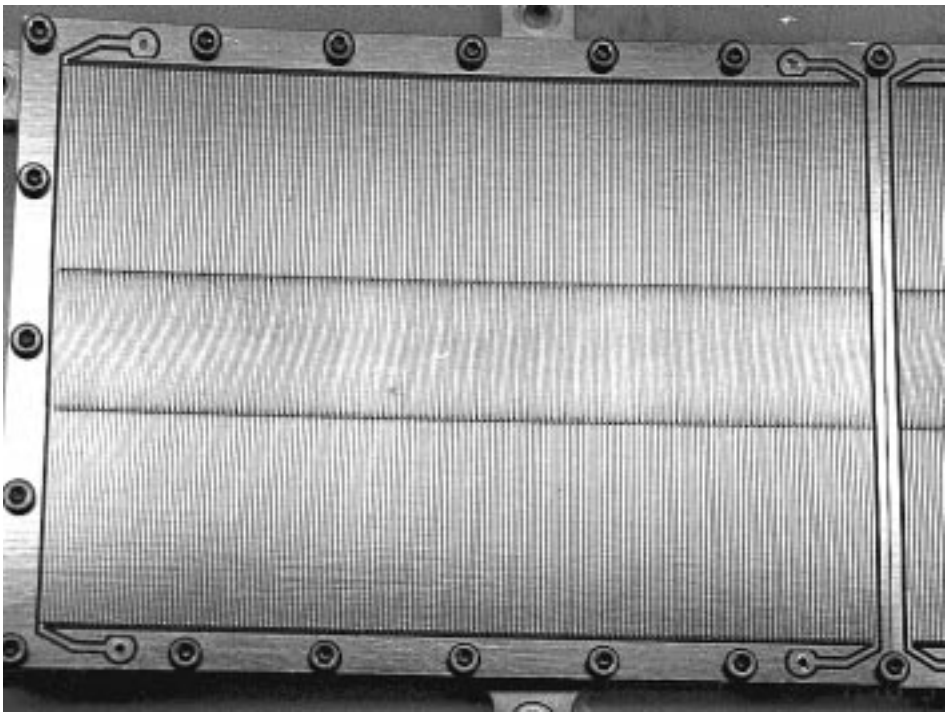

Figure 3. One segment of the two helical double delay line anodes used for each FUSE detector, showing the 90mm x 15mm active area and the upper and lower helical delay line top surface conductors.

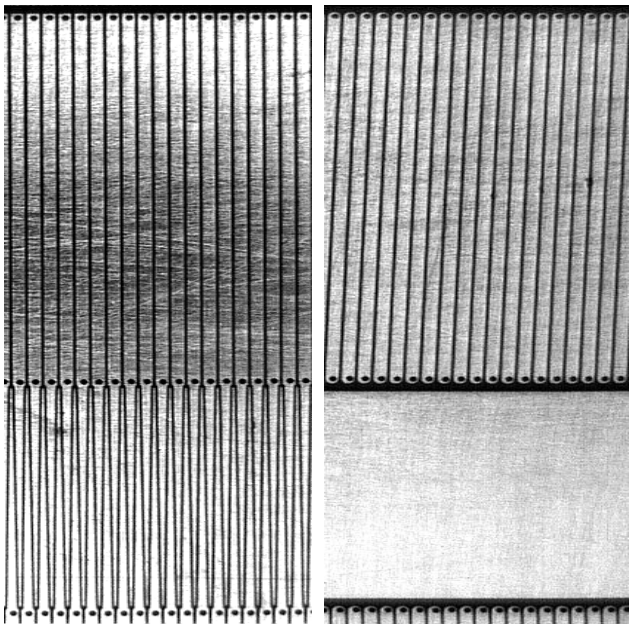

Top side Bottom side

Figure 4. A section of a helical double delay line anode showing the interleaved wedges in the active area and the upper and lower parts of the helical delay line

conductors connected by plated through holes.

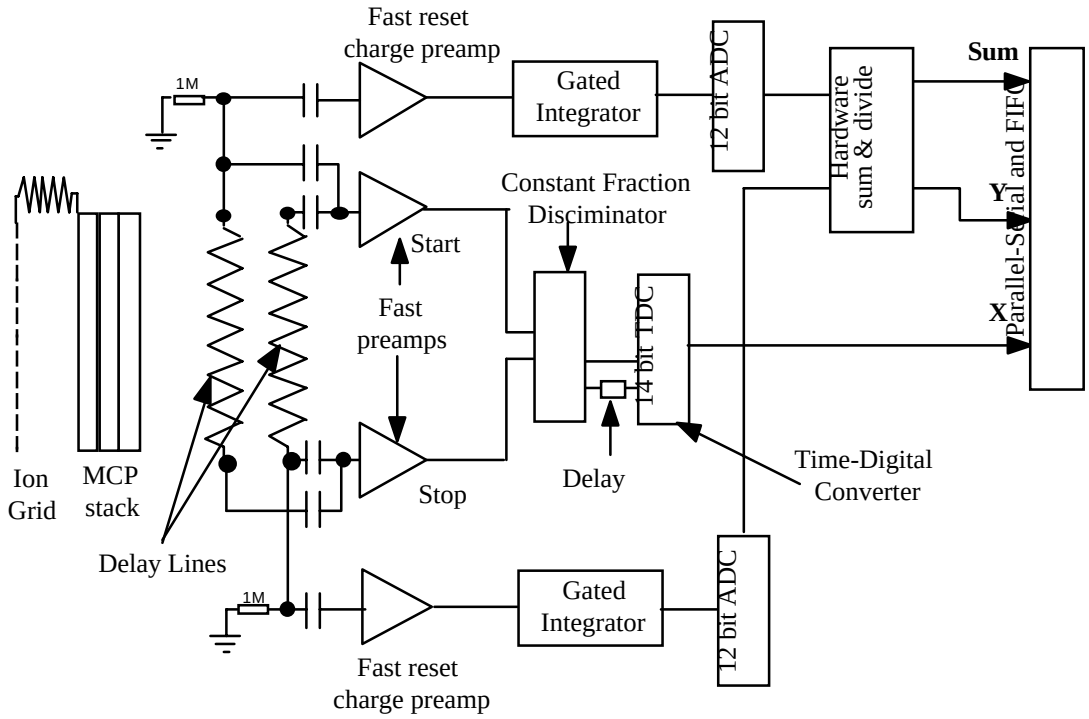

Figure 5. Event position encoding electronics block diagram

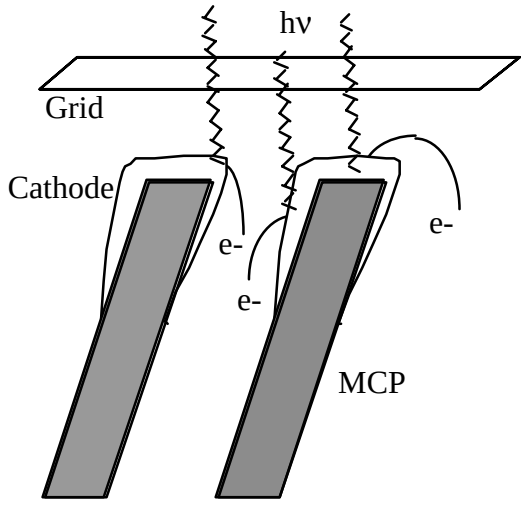

Figure 6. Opaque KBr photocathode configuration on MCP with bias grid.

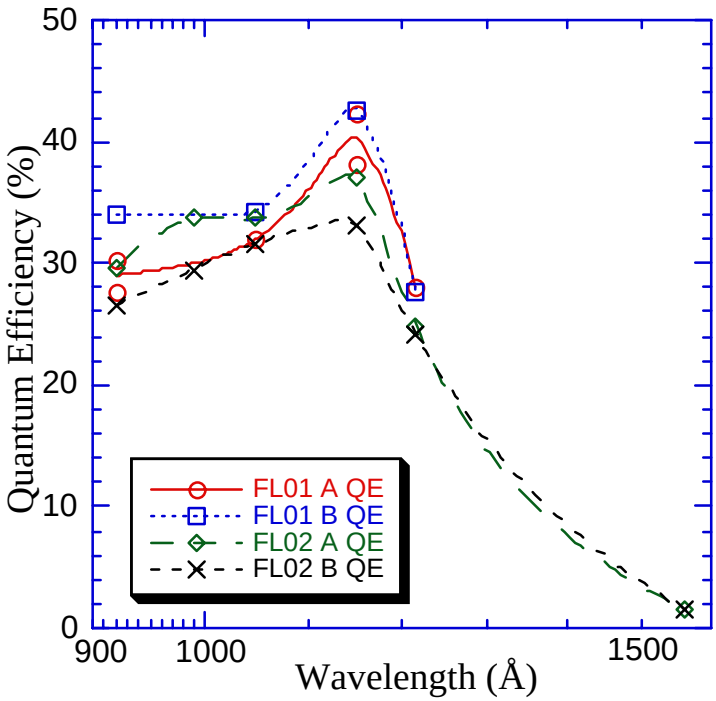

Figure 7. Measured flight detector KBr photocathode quantum detection efficiency for FL01 & FL02.

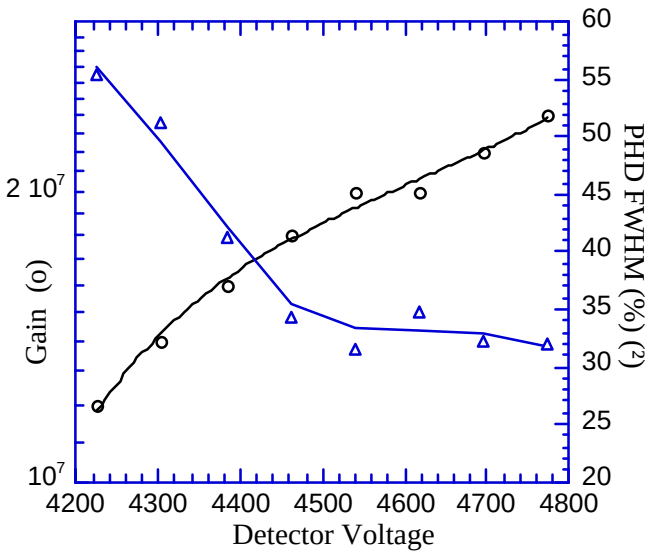

Figure 8. Gain and PHD as a function of voltage for FL03B, UV (2537Å) full flood.

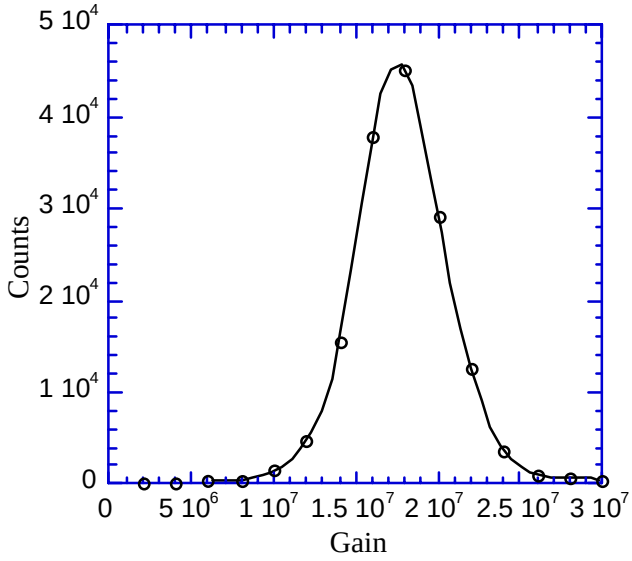

Figure 9. PHD for FL03B, UV (2537Å) full flood (32% FWHM).

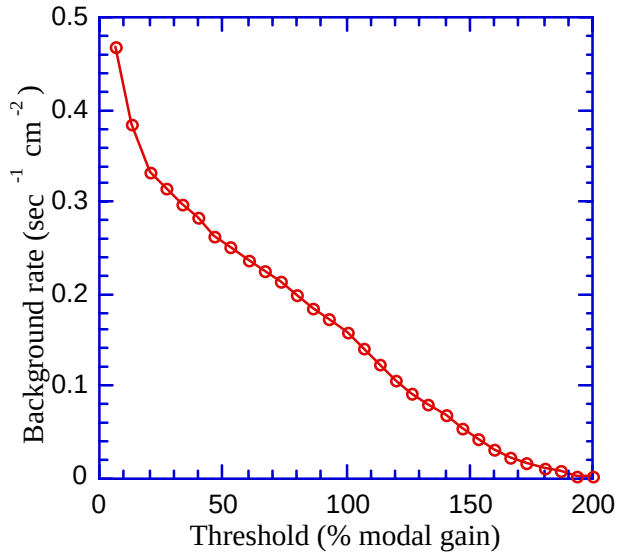

Figure 10. FL02 background rate as a function of counting threshold.

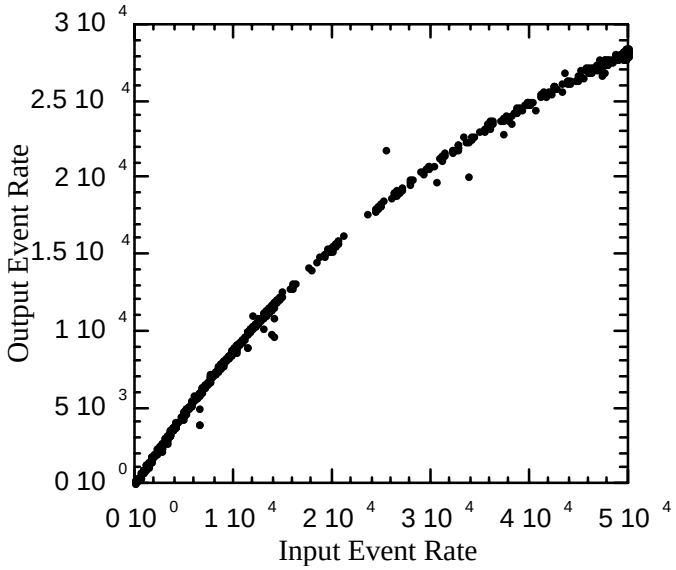

Figure 11. Flight electronics dead time curve comparing the output/input event rate

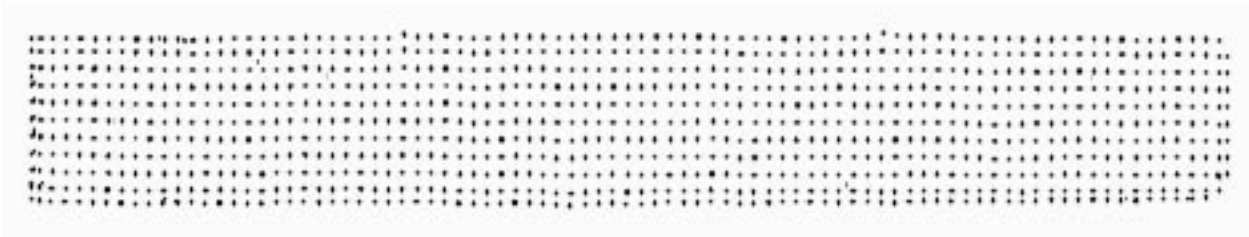

Figure 12. Pinhole mask image for FL02, 8.6cm x 1cm with 1mm pinhole period, 10µm holes.

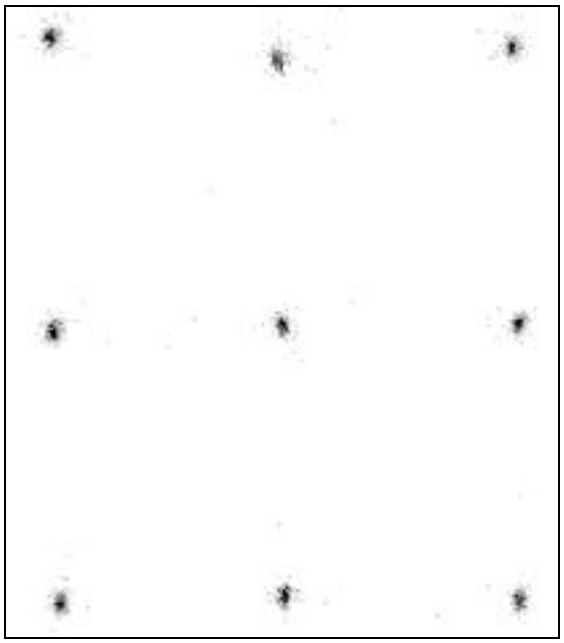

Figure 13. Image section showing nine of the pinhole images from Figure 12.

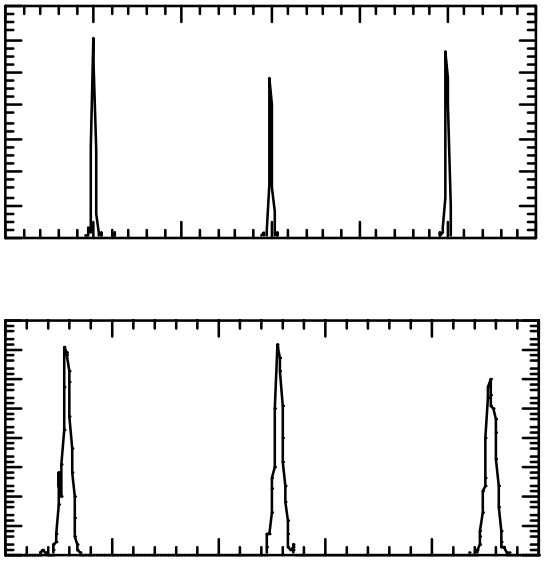

Figure 14. X and Y image histograms of the center row & column of Figure 12.

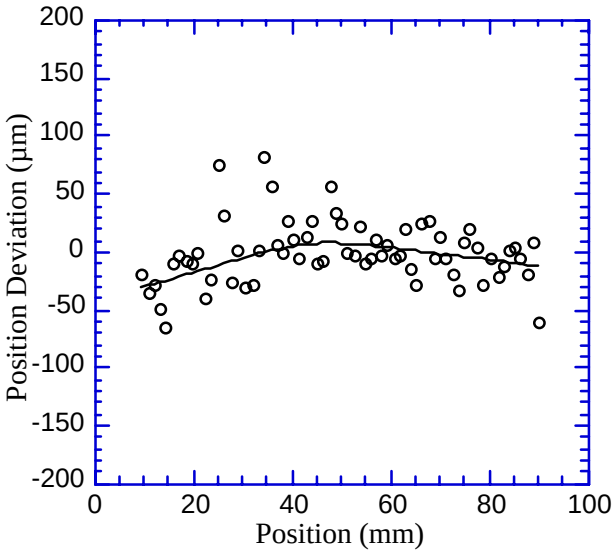

Figure 15. Image linearity as a function of position for pinhole images in Figure 12.

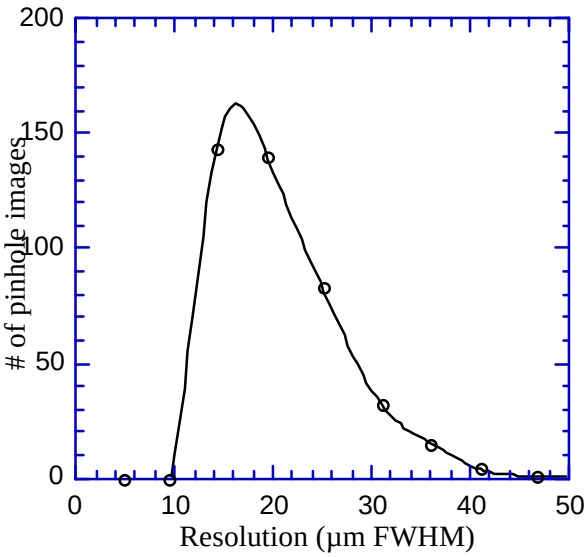

Figure 16. X resolution histogram for FL03 showing the distribution of spot image widths.

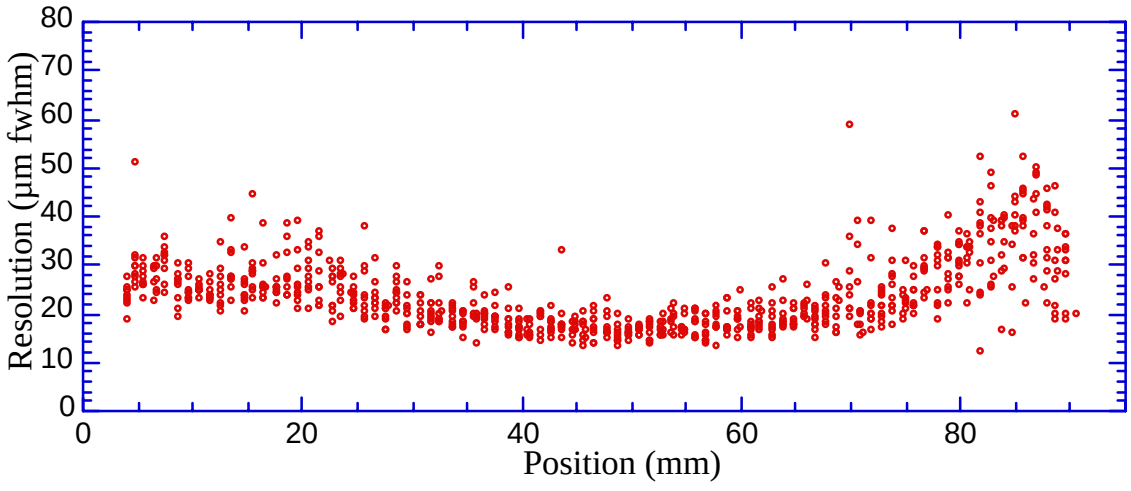

Figure 17. FL03 pinhole image width as a function of X position for all pinhole images.

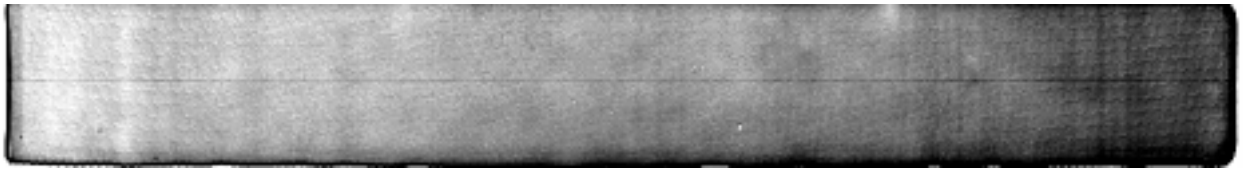

Figure 18. Full field illumination intensity map for FL01 showing the MCP multifibers.

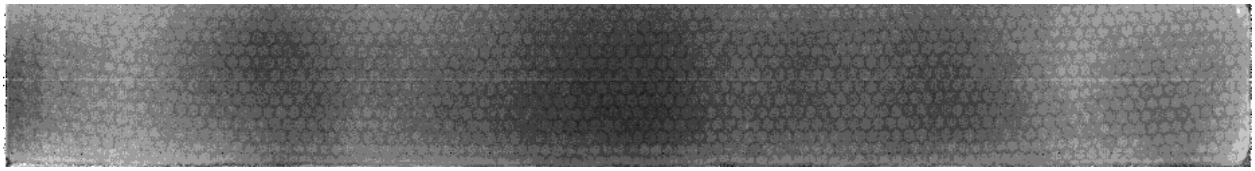

Figure 19. Gain map for FL01, showing the gain variations at the MCP multifibers.

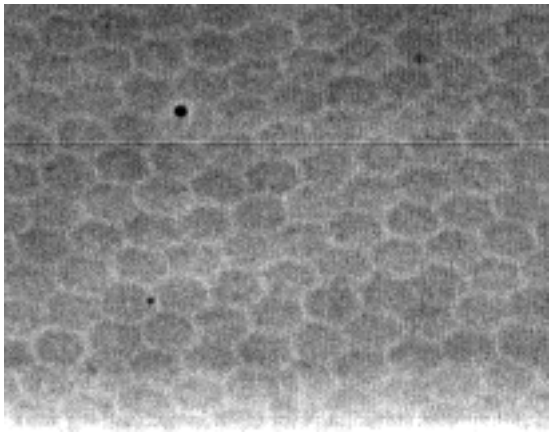

Figure 20. High resolution image section for FL02 showing multifiber modulation.

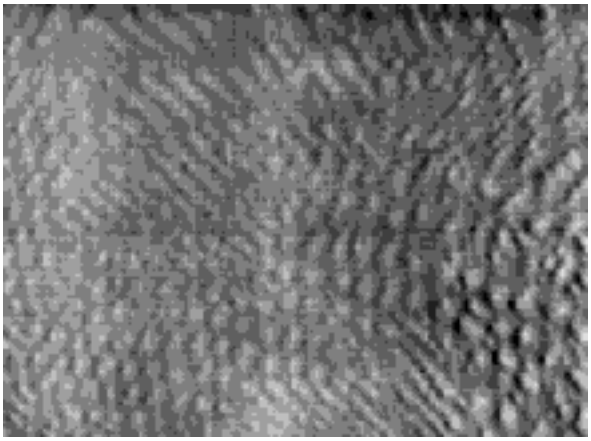

Figure 21. High resolution image section for a non-flight 10μm pore MCP stack.

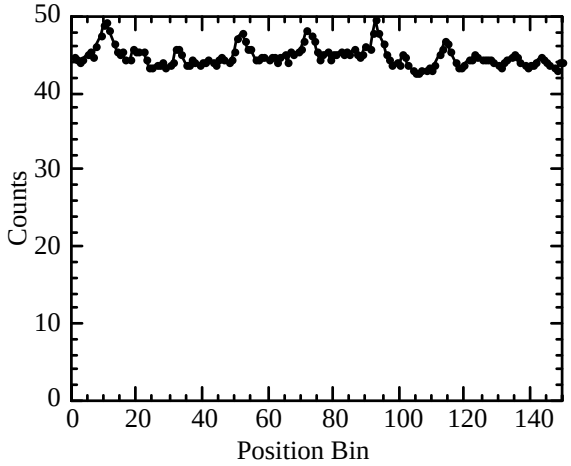

Figure 22. Histogram section of Fig. 20 showing the small multifber modulation

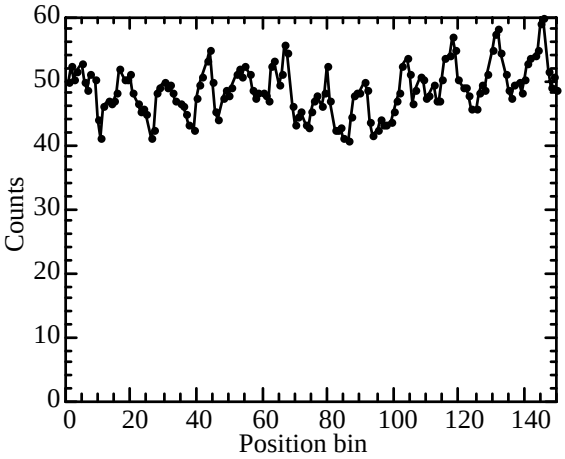

Figure 23. Histogram section of Fig. 21 showing periodic Moire modulation.